OUKA
The University of Osaka
Institutional Knowledge Archive

Title	Microalgae-Mediated Synthesis of Functionalized Gold Nanoparticles with High Photothermal Stability
Author(s)	Hamida, Reham Samir; Sotoma, Shingo; Kah, James Chen Yong et al.
Citation	ACS Sustainable Chemistry and Engineering. 2025, 13(45), p. 19599-19612
Version Type	VoR
URL	https://hdl.handle.net/11094/105857
rights	This article is licensed under a Creative Commons Attribution 4.0 International License.
Note	

The University of Osaka Institutional Knowledge Archive : OUKA

https://ir.library.osaka-u.ac.jp/

The University of Osaka

ACS Sustainable Chemistry & Engineering

pubs.acs.org/journal/ascecg

Open Access

This article is licensed under CC-BY 4.0

Research Article

Microalgae-Mediated Synthesis of Functionalized Gold Nanoparticles with High Photothermal Stability

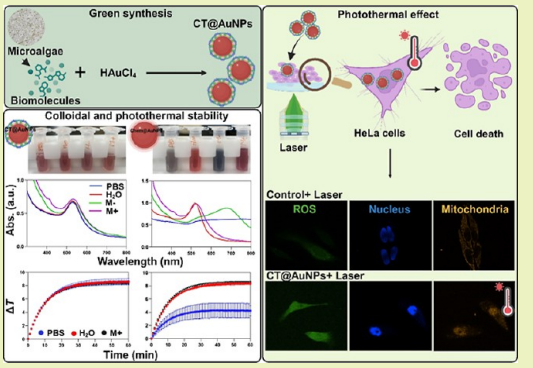
Reham Samir Hamida, Shingo Sotoma, James Chen Yong Kah, Yoshie Harada, and Madoka Suzuki*

Cite This: *ACS Sustainable Chem. Eng.* 2025, 13, 19599−19612

Read Online

ACCESS | Metrics & More | Article Recommendations | Supporting Information

ABSTRACT: Gold nanoparticles (AuNPs) exhibit localized surface plasmon resonance (LSPR) and are promising photothermal agents. However, the aggregation susceptibility and poor colloidal stability limit their biomedical applications, particularly in photothermal therapy. Here, a one-pot green method is employed to synthesize AuNPs using aqueous extracts of *Coelastrella thermophila* (CT) and *Arthrospira* sp. (SP) as reducing and stabilizing agents. These biogenic AuNPs (CT@AuNPs and SP@AuNPs), and their counterpart synthesized using a conventional procedure (Chem@AuNPs) have quasi-spherical shapes with hydrodynamic diameters of 26.8 ± 10.3, 19.2 ± 6.1, and 11.4 ± 3.3 nm, respectively, and negatively charged surfaces. Fourier transform infrared spectroscopy reveals that CT@AuNPs and SP@AuNPs feature surface functional groups derived from algal proteins, carbohydrates, and fatty acids, which are associated with their greater colloidal stability (48 h) than Chem@AuNPs. These AuNPs elevate solution temperature up to ∼8 °C under continuous green laser irradiation for 1 h. Cytotoxicity of CT@AuNPs and SP@AuNPs was lower toward Vero cells than toward HeLa cells, and under our experimental conditions, they induced cell death in ∼70% of the latter upon green laser irradiation. Analyses using the 2′,7′-dichlorodihydrofluorescein diacetate and morphology suggest that the AuNP-induced cell death is attributed to LSPR-mediated hyperthermia and reactive oxygen species. Our alternative route to stable AuNPs addresses the persistent challenges posed by conventionally synthesized AuNPs in photothermal therapy and other fields.



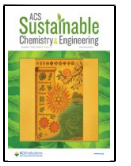
KEYWORDS: *green synthesis, colloidal stability, photothermal stability, reactive oxygen species, surface modification*

INTRODUCTION

Gold nanoparticles (AuNPs) are one of the most widely used metallic nanoparticles (NPs) in biomedical applications, including therapeutic, drug delivery, bioimaging, sensing, and theranostic applications due to their versatile properties. These properties include a high surface-to-volume ratio, easy surface functionalization, remarkable optical properties, and low toxicity.[1−5] The localized surface plasmon resonance (LSPR) exhibited by AuNPs enables efficient local heat release upon their excitation with light and makes them promising photothermal therapy (PTT) agents,[6,7] as the released heat can damage neighboring malignant cells.[8−10] Several types of AuNPs, including nanospheres,[11] nanorods,[6] and nanocomposites (e.g., Au−silica nanoshells[2] and Au−Fe oxide NPs[12]), have been identified as effective photothermal agents for hyperthermic cancer treatment. Despite the advantages of AuNPs, their practical industrial and medical applications are constrained by their interfacial properties, which result in a low colloidal stability and high aggregation propensity.[13,14] Surface modification is often required to mitigate aggregation; however, the corresponding reactants are often toxic, and the resulting byproducts may exert undesirable environmental effects.[14,15] Therefore, alternatives to conventional AuNP synthesis methods are highly sought after.

Over the past decade, green approaches have become a popular and reliable alternative for synthesizing metal NPs because of their sustainability, simplicity, and scalability.[16−19] Microalgae-mediated NP synthesis relies on algal biomolecules (e.g., proteins, carbohydrates, and fatty acids) as reducing and stabilizing agents, making it particularly promising.[17,20] Green methods provide access to NPs with diverse shapes and sizes, resulting in time, energy, and cost savings while providing the additional benefits of surface functionalization and high stability.[11,21−23] Most studies on the green synthesis of AuNPs simply demonstrate their formation and report their properties, and the optimization of the corresponding reaction parameters, which influence the AuNP shape, functionality and stability, is therefore underexplored.[11] Thus, a deep under-

Received: July 27, 2025
Revised: October 11, 2025
Accepted: October 13, 2025
Published: November 7, 2025



ACS Publications

© 2025 The Authors. Published by American Chemical Society

https://doi.org/10.1021/acssuschemeng.5c07786
ACS Sustainable Chem. Eng. 2025, 13, 19599−19612

Downloaded from http://pubs.acs.org/ascecg/article-pdf/13/45/19599/4245742/sc5c07786.pdf by UNIV OF OSAKA user on 27 July 2026

standing of factors governing the colloidal stability and optical properties of AuNPs would fill an important knowledge gap and facilitate the translation of biogenic AuNPs into various applications, including biomedical ones.[24]

We selected *Coelastrella thermophila* (CT), a novel thermotolerant microalga with unique lipid and antioxidant profiles, to explore for the first time its reduction potential to produce AuNPs. *Coelastrella* sp.[25] is known to be rich in organic molecules with reduction potentials, which can reduce precursors into NPs.[26] As a comparison, *Arthrospira* sp.[27] (SP), a cyanobacterium approved by the Food and Drug Administration (FDA), was used. Previous studies have shown that this strain possesses potent reductive biomolecules, such as phycocyanin and polysaccharides, and exhibits potential for the synthesis of AuNPs.[28] Accordingly, in the present study, aqueous extracts of *C. thermophila* and *Arthrospira* sp. were used to prepare AuNPs (CT@AuNPs and SP@AuNPs, respectively) without the addition of stabilizers. The present study extends the biogenic AuNPs platform by providing a detailed investigation into their photothermal properties and in vitro biological effects.

EXPERIMENTAL SECTION

Chemicals. $HAuCl_4{\cdot}4H_2O$ (17302-01), trisodium citrate dihydrate (31405-05), and dimethyl sulfoxide (09659-85) were purchased from Nacalai Tesque (Kyoto, Japan). *Arthrospira* sp. powder (CGN-01224) was purchased from California Gold Nutrition (Perris, USA). The DNA extraction kit (NA2012-01) was purchased from Attogene (TX, USA). Dulbecco's Modified Eagle Medium (DMEM, 11965-092), phosphate-buffered saline (PBS, 10010-0223), trypsin (TryplE Express, 12605-010), fetal bovine serum (FBS, 26140-079), penicillin and streptomycin (15140-122), trypan blue (15250-061), the 3-(4,5-dimethylthiazol-2-yl)-2,5-diphenyltetrazolium bromide (MTT kit, M6494), and MitoTracker Red (M7513) were purchased from Thermo Fisher Scientific (MA, USA). Advantec filter paper (No. 2, 150 mm) was purchased from Toyo Roshi Kaisha Ltd. (Tokyo, Japan). Glass beads (18406-500G) and 2′,7′-dichlorodihydrofluorescein diacetate (DCFH-DA, D6883-50MG) were purchased from Sigma-Aldrich (MO, USA). The Hoechst stain (ab228550) was purchased from Abcam (Cambridge, UK).

Isolation and Identification of Microalgae. A specimen collected from the sand of Riyadh (Saudi Arabia) was placed in a 50 mL sterilized centrifuge tube, transported to the laboratory, and maintained in a Petri dish containing a sterilized BG11 medium under a fluorescent lamp (2000 ± 200 lx, 12 h/12 h dark/light cycle) at room temperature for a week. A serial dilution method was used to purify the samples according to the protocol of Bolch et al.[29] The purified sample was cultured in a sterilized BG11 medium (1000 mL) inside a flask connected to an air agitation system under the same growth conditions. A 10 μL aliquot of the suspension was placed on a glass slide and covered with a coverslip, and the morphology of the microalgae was examined using an inverted light microscope (Nikon Eclipse Ts2, Tokyo, Japan). Genomic DNA was extracted using a DNA extraction kit according to the manufacturer's instructions. The polymerase chain reaction (PeqSTAR 96X universal gradient thermal cycler, VWR, Germany) was used to amplify DNA according to the method of Khaw et al.[30] with some modifications: The initial denaturation was performed at 94.5 °C (gradient ramping range = 0.5 °C) for 6 min and followed by 40 cycles of 95 °C for 30 s (denaturation step), 52 °C for 1 min (annealing step), and 74 °C for 1 min (extension), with the final extension performed at 72 °C for 10 min. CCTGGTTGATCCTGCCAG and TTGATCCTTCTGCAGGTTCA were used as the forward and reverse primers, respectively for amplification. Amplicons were stored in nuclease-free water and sent to Macrogen (Seoul, South Korea) for sequence analysis.

Preparation and Phytochemical Composition Analysis of Algal Extracts. The algal extracts were prepared from a microalga (*C. thermophila*) and a cyanobacterium (*Arthrospira* sp.). After 15 days of culturing *C. thermophila*, 5000 mL of the algal suspension was centrifuged (Himac CF15RN, Hitachi, Ibaraki, Japan) at 4800*g* for 10 min. The pellets were washed at least three times using Milli-Q water, kept at −80 °C overnight, and freeze-dried (FDU-12AS, AS ONE Corp., Osaka, Japan) for 24 h. The dried powder was vortexed with glass beads for 1−2 min to obtain a fine powder. *C. thermophila* (200 mg) and *Arthrospira* sp. (2 g) powders were separately dissolved in Milli-Q water (100 mL) and kept in a water bath (Thermo minder SH-12, TAITEC, Saitama, Japan) at 60 °C for 30 min. The mixtures were then cooled to room temperature and centrifuged at 16,700*g* for 10 min. The supernatant was filtered through Advantec filter paper (No. 2) to remove debris. Both extracts were used for NP synthesis as described below. The phytochemical compositions of the extracts were analyzed using a Trace GC-TSQ mass spectrometer (Thermo Fisher Scientific) with a TG-5MS direct capillary column (30 m length × 0.25 mm inner diameter × 0.25 μm film thickness) as described elsewhere.[31]

Synthesis of Chem@AuNPs. Chem@AuNPs were synthesized as described by Sotoma and Harada.[14] Aqueous $HAuCl_4$ (1.2 mL, 10 mM) was added to Milli-Q water (50 mL), and the solution was heated to 95 °C in an oil bath upon stirring at 200 rpm. Then, aqueous trisodium citrate dihydrate (1.13 mL, 10 mg/mL) was added, and the mixture was refluxed and stirred for 15 min, which resulted in a color change from dark violet to purple and ruby red over 15 min. This color change suggested the formation of citrate-coated AuNPs. The Chem@AuNP suspension was cooled upon stirring for 15 min before further use.

Optimization of CT@AuNP and SP@AuNP Syntheses. The optimized parameters were the algal extract/$HAuCl_4$ ratio (V_{mL}/V_{mL}), $HAuCl_4$ concentration, reaction temperature, reaction time, and pH. Initially, the influence of the algal extract/$HAuCl_4$ ratio on the size and stability of CT@AuNPs and SP@AuNPs was investigated by mixing *C. thermophila* and *Arthrospira* sp. extracts with 0.5 mM $HAuCl_4$ at ratios of 1:1, 1:2, 1:4, and 1:9 at 95 °C for 15 min without adjusting pH (initial pH). After incubation, the absorption spectrum of the AuNP suspension was measured using an ultraviolet-visible (UV−vis) spectrophotometer (V-560, JASCO, Tokyo, Japan) in the region of 200−800 nm with a resolution of 1 nm. The effect of $HAuCl_4$ concentration on the AuNP size and stability was assessed by mixing 0.5 or 1 mM $HAuCl_4$ with *C. thermophila* and *Arthrospira* sp. extracts at the optimized ratio (1:1 and 1:9 for CT@AuNPs and SP@AuNPs, respectively) and 95 °C/initial pH for 15 min. The effect of the reaction temperature (40, 60, 80, and 95 °C) was examined at the optimized concentration (0.5 mM for both CT@AuNPs and SP@AuNPs) and algal extract/$HAuCl_4$ ratio. The effect of the reaction time was examined by heating the reaction mixture for 15, 30, and 60 min under the above-mentioned optimal conditions. The effects of pH were investigated by adjusting the pH of the algal extract/$HAuCl_4$ mixture to 3.4 (initial pH), 6, 7, 8, or 12 and performing the reaction under the above-mentioned optimal parameters.

Characterization of AuNPs. The UV−vis absorption spectra of CT@AuNPs, SP@AuNPs, and Chem@AuNPs were measured for 1 mL samples in the range of 200−800 nm at a resolution of 1 nm. The surface functional groups of CT@AuNPs, SP@AuNPs, and Chem@AuNPs and biomolecules in *C. thermophila* and *Arthrospira* sp. extracts were determined using the Fourier transform infrared (FTIR) attenuated total reflection spectroscopy (ALPHA spectrometer, Bruker, MA, USA) in the range of 400−4000 cm^{-1}. The zeta potentials and hydrodynamic diameters (HDs) of CT@AuNPs, SP@AuNPs, and Chem@AuNPs were measured using a Malvern zetasizer (Zetasizer Nano ZSP, Malvern Instruments Limited, Worcestershire, UK). The AuNP suspension (1 mL) was centrifuged at 21,600*g* for 30 min, and the pellet was washed with Milli-Q water more than three times and suspended in 1 mL of the same. The suspension was sonicated using a water bath sonicator (VS-100-III, AS ONE) for 15 min, diluted 10-fold with Milli-Q water, and subjected to measurements. The NP size and shape were examined by transmission

Downloaded from http://pubs.acs.org/ascecg/article-pdf/13/45/19599/4245742/sc5c07786.pdf by UNIV OF OSAKA user on 27 July 2026

https://doi.org/10.1021/acssuschemeng.5c07786
ACS Sustainable Chem. Eng. 2025, 13, 19599−19612

electron microscopy (TEM, H-7650, Hitachi High-Tech Corporation, Tokyo, Japan) at 120 kV. To prepare the grid for TEM imaging, the NP suspension (1 mL) was centrifuged at 21,600*g* for 30 min, washed three times with Milli-Q water and one time with ethanol, and rinsed with Milli-Q water (1 mL). The samples were sonicated for 1 min, loaded onto a carbon-coated copper grid (400 mesh, Electron Microscopy Sciences, PA, USA), and air-dried in a laminar flow cabinet. The particle sizes in the TEM micrographs were measured using the ImageJ software (National Institutes of Health, Bethesda, MD, USA). The crystal structures of CT@AuNPs and SP@AuNPs were analyzed by X-ray diffraction (XRD, D8 DISCOVER, Bruker), with patterns recorded in the 2θ range of 0°−80° using Cu K_α radiation at 30 kV/30 mA and a scan rate of 4°/min.

Colloidal Stability Evaluation. The colloidal stabilities of CT@AuNPs, SP@AuNPs, and Chem@AuNPs in various systems, including Milli-Q water, PBS, and phenol red−free DMEM with (M+) and without (M−) 10% FBS, were assessed as follows. The AuNP suspension (1 mL) was centrifuged at 21,600*g* for 30 min, the supernatant was discarded, and the pellet was washed with Milli-Q water and dispersed in 1 mL of the desired medium. The sample was vortexed for 1 min and incubated at ambient temperature for 1, 18, 24, and 48 h. After incubation, the samples were sonicated for 60 s using a Handy Sonic UR-20P probe (Tomy Seiko Co, Tokyo, Japan), and their absorption spectra were recorded as described above. The HDs of CT@AuNPs, SP@AuNPs, and Chem@AuNPs were measured in Milli-Q water, PBS, M+, and M− after incubation for 1 and 24 h as described above. Prior to measurements, the incubated samples were sonicated for 15 min and diluted 10-fold.

Photothermal Efficiency and Stability Evaluation. The photothermal efficiencies and stabilities of CT@AuNPs, SP@AuNPs, and Chem@AuNPs under green laser irradiation (532 nm; Sapphire SF532, Coherent, PA, USA) were determined. This wavelength overlaps the LSPR absorption of the synthesized AuNPs and enables efficient photothermal conversion. The temperatures of CT@AuNP, SP@AuNP, and Chem@AuNP suspensions (1 mL) in Milli-Q water, PBS, and M+ and those of the controls, namely Milli-Q water, PBS, M+, $HAuCl_4$, and the aqueous extracts of *C. thermophila* or *Arthrospira* sp. were monitored using a K-type thermocouple and recorded by a data logger (GL10-TK, Graphtec Corporation, Yokohama, Japan). The temperature change (ΔT) was calculated as $\Delta T = T_E - T_i$, where T_i is the initial temperature, i.e., the average temperature of the solutions held at room temperature for 1 min before irradiation, and T_E is the suspension temperature during irradiation with the green laser at 100 mW, 0.7 mm in diameter (~26 W/cm^2), for 15 min. The influence of NP concentration on photothermal efficiency was examined by exposing CT@AuNP, SP@AuNP, and Chem@AuNP suspensions with various concentrations (20, 40, 160, and 600 μg/mL) to the green laser (100 mW, 0.7 mm in diameter) for 15 min. Similarly, the influence of laser power (30, 60, and 100 mW) on photothermal efficiency was conducted by irradiating aqueous suspensions of CT@AuNPs, SP@AuNPs, and Chem@AuNPs (40 μg/mL) for 15 min. In the photothermal stability assay, CT@AuNP, SP@AuNP, and Chem@AuNP suspensions in Milli-Q water, PBS, and M+ (40 μg/mL, 1 mL) were irradiated at 100 mW for 60 min.

Cytotoxicity Evaluation. HeLa and Vero cells were grown using culture medium (DMEM supplemented with 10% FBS, 100 U/mL penicillin and 100 μg/mL streptomycin) and kept in an incubator (MCO-18A1C, SANYO, Osaka, Japan) at 37 °C under 5% CO_2. At 75% confluency, the cells were passaged using trypsin, counted, seeded (5×10^3 cells/well) into 96-well plates, and kept for 24 h under the same conditions. The cytotoxicities of CT@AuNPs, SP@AuNPs, and Chem@AuNPs toward the two cell types were assessed using the MTT assay. AuNPs of the desired type (40 μg) were suspended in culture medium (1 mL), and the mixture was sonicated for 30 min to achieve a uniform particle dispersion. The cells were then incubated with AuNP suspensions of different concentrations (5, 10, 20, and 40 μg/mL) at 37 °C for 24 h. After 24 h, the medium was discarded and replaced with a fresh culture medium (100 μL/well) and 5 mg/mL MTT solution (10 μL/well). The plates were kept at 37 °C for 3 h. After incubation, the medium was discarded, and dimethyl sulfoxide (100 μL/well) was added to dissolve formazan crystals. The plates were then kept on a shaker (400 rpm, MTS 2/4, IKA, Staufen, Germany) for 15 min at room temperature. The absorbance at 570 nm of each well was measured using a plate reader (Multiskan Sky 1530, Thermo Fisher Scientific).[32] Cell viability (%) was estimated as 100% × absorbance (treated)/absorbance (control).

In Vitro Photothermal Efficacy Evaluation. The photothermal efficacy of AuNPs against HeLa cells was estimated in vitro using an in-house-built system. HeLa cells (1×10^4) were seeded in 35 mm−diameter glass dishes and incubated for 48 h until a confluency of 60%. Four groups were established, namely untreated HeLa cells (Gr1), HeLa cells laser-irradiated (Gr2), HeLa cells treated with 40 μg/mL CT@AuNPs or SP@AuNPs or Chem@AuNPs (Gr3), and HeLa cells treated with 40 μg/mL CT@AuNPs or SP@AuNPs or Chem@AuNPs and laser-irradiated (Gr4). The AuNP suspensions were prepared by suspending AuNPs (40 μg) in culture medium (1 mL) and sonicating for 30 min. After 48 h, the old medium in the plates was discarded, 40 μg/mL CT@AuNPs, SP@AuNPs, or Chem@AuNPs was added (2 mL), and the cells were incubated for 3 h. Subsequently, the old medium was discarded, the cells were washed with PBS, and a fresh culture medium was added. Gr2 and Gr4 were exposed to the green laser (100 mW, 2.1 mm in diameter; i.e., ~3 W/cm^2) for 15 min. All plates in all groups were incubated in a CO_2 incubator at 37 °C for 24 h for further applications.[33]

Trypan Blue Staining. After 24 h, the old medium was discarded, and the cells were washed with PBS and then mixed with 2 mL of a trypan blue solution (1 mL)−DMEM (1 mL) mixture. The plates were incubated in a CO_2 incubator at 37 °C for 5 min. The dye solution was discarded, the cells were washed twice with PBS, and a fresh culture medium (1 mL) was added. The cells were imaged using an inverted light microscope at magnifications of 10×. A similar experiment was conducted to count the cells using a cell counter (LUNA-III, Logos Biosystems, Gyeonggi-do, South Korea). HeLa cells (1×10^4) were seeded in 96-well plates and kept in the CO_2 incubator at 37 °C for 24 h. Subsequently, the old medium was discarded, the NP suspension (100 μL/well) was added, and the plates were incubated for 3 h. After 3 h, the old medium was discarded, and a fresh culture medium (100 μL/well) was added. The cells in Gr2 and Gr4 were exposed to the green laser. All plates in all groups were incubated in the CO_2 incubator at 37 °C for 24 h. Subsequently, the old medium was discarded, the cells were washed with PBS, trypsin (100 μL/well) was added, and the cells were incubated at 37 °C for 4 min. To neutralize trypsin, culture medium (100 μL/well) was added, and the cell suspension was collected in Eppendorf tubes. Then, the cell suspensions (20 μL) were mixed with 20 μL of the trypan blue−DMEM mixture in a 1:1 ratio (v/v) and incubated at 37 °C for 5 min; the cells were subsequently counted.[34]

Detection of Intracellular Reactive Oxygen Species. Intracellular reactive oxygen species (ROS) were detected in HeLa cells before and after treatment with AuNPs and laser exposure using a DCFH-DA and laser confocal microscopy. The old medium in all groups was discarded after 24 h of incubation, the cells were washed with PBS, and 500 μL of culture medium containing DCFH-DA (20 μM) was added. The cells were then incubated at 37 °C for 30 min. Following incubation, the solution was discarded, the cells were washed with PBS, and culture medium (1 mL) was added. The cells were then imaged using a confocal fluorescence microscope (AX R, with PLAN APO λD 60×, oil, Nikon).[35]

Confocal Fluorescence Microscopy Imaging. Morphological changes in nuclei and mitochondria were determined using double staining with Hoechst and MitoTracker Red, respectively. After 24 h of incubation, the cells were washed with PBS after removing the old medium, 500 μL of DMEM containing 1 μL of MitoTracker Red (10 μM) and 0.5 μL of Hoechst (20 mM) was added, and the cells were incubated for 5 min. After 5 min, the medium was discarded, the cells were washed with PBS, a fresh culture medium was added, and the cells were imaged using the above-mentioned confocal fluorescence microscope.

Downloaded from http://pubs.acs.org/ascecg/article-pdf/13/45/19599/4257742/sc5c07786.pdf by UNIV OF OSAKA user on 27 July 2026

https://doi.org/10.1021/acssuschemeng.5c07786
ACS Sustainable Chem. Eng. 2025, 13, 19599−19612

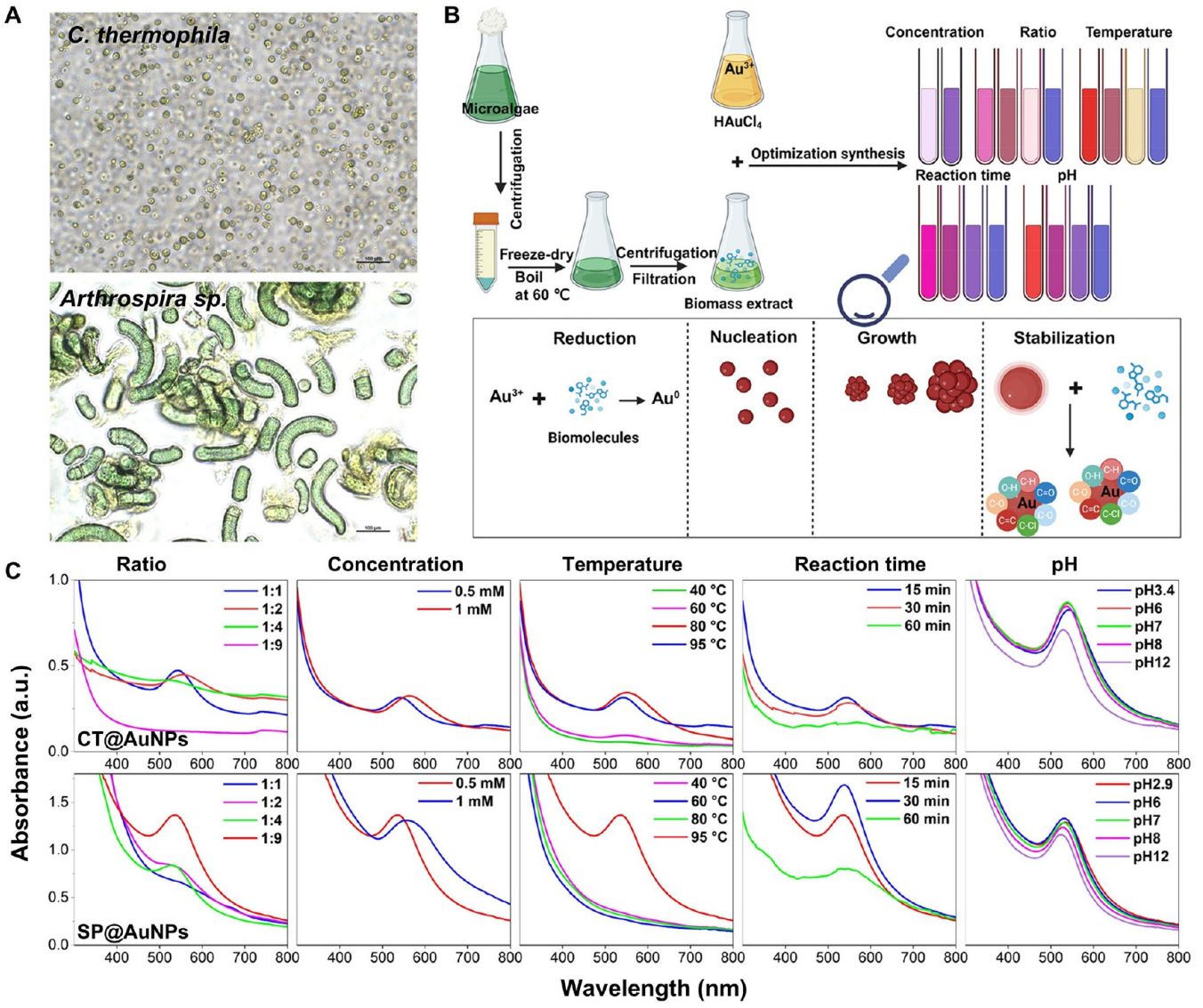


Figure 1. (A) Optical microscopy images of the *Coelastrella thermophila* var. *globulina* isolate FACHB-2308 (top) and *Arthrospira* sp. (bottom). (B) Schematic and (C) optimization of CT@AuNP (top) and SP@AuNP (bottom) syntheses. CT@AuNP and SP@AuNP refer to gold nanoparticles prepared using *C. thermophila* var. *globulina* isolate FACHB-2308 and *Arthrospira* sp. extracts, respectively.

Statistical Analysis. GraphPad Prism v.9.3.1 (GraphPad Software Inc., San Diego, CA, USA), Origin 2023b (OriginLab Corporation, Northampton, MA, USA), and ImageJ were used for data analysis. Experiments were performed in triplicate, and the results were reported as the corresponding means ± standard deviations unless stated otherwise.

RESULTS

Identification of Algal Strains. Microalgae were isolated from the sand of Riyadh (Saudi Arabia), and *Arthrospira* sp. was purchased from a commercial supplier as an identified and FDA-approved cyanobacterium strain. 18S rRNA sequencing was performed to identify the novel microalgal strain, and a phylogenetic tree was constructed to assess the taxonomic relationships among the closely related microalgal strains. The isolated strain was 96.66% identical to the *C. thermophila* var. *globulina* isolate FACHB-2308 with a 100% query cover. The sample sequence was deposited in NCBI (accession number OR782203). According to the obtained phylogenetic tree, the isolated strain was clustered within *Coelastrella* and *Asterarcys* sp. and grouped closely with the FACHB-2308 isolate, featuring a strong bootstrap support of 99% (Figure S1). The morphologies of the FACHB-2308 isolate and *Arthrospira* sp. were examined using optical microscopy. The FACHB-2308 isolate appeared olive green and featured (sub) spherical young cells, whereas mature cells had approximately spherical shapes with intracellular vacuoles (Figure 1A). The cells had parietal cup-shaped chloroplasts with distinct pyrenoids. *Arthrospira* sp. appeared as fragmented, curved, and segmented blue-green filaments (Figure 1A). The volatile metabolites of *C. thermophila* and *Arthrospira* sp. extracts were analyzed using gas chromatography−mass spectrometry (GC−MS; Figure S2 and Table S1). The profile of the *C. thermophila* extract featured two main peaks at 26.6 and 29.7 min, which were identified as palmitic acid (47.5%) and oleic acid (19.8%), respectively. The profile of the *Arthrospira* sp. extract featured two dominant peaks at 26.7 and 29.8 min, identified as palmitic acid (23.6%) and linoleoyl chloride (31.5%), respectively, and a minor peak of methyl oleate (10%) at 29.0 min.

https://doi.org/10.1021/acssuschemeng.5c07786
ACS Sustainable Chem. Eng. 2025, 13, 19599−19612

Downloaded from http://pubs.acs.org/ascecg/article-pdf/13/45/19599/4245742/sc5c07786.pdf by UNIV OF OSAKA user on 27 July 2026

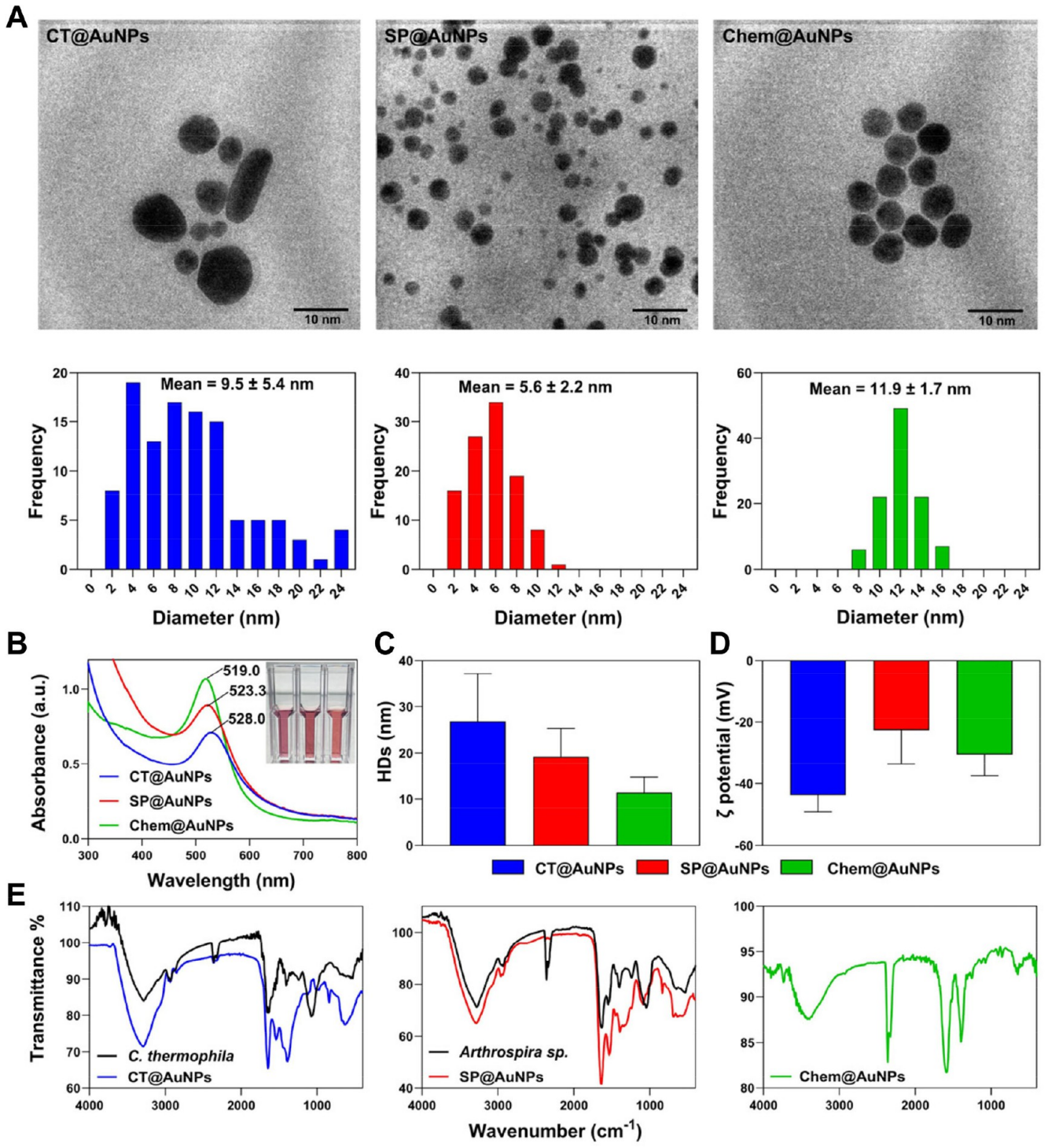


Figure 2. Properties of CT@AuNPs and SP@AuNPs synthesized under optimal conditions, and gold nanoparticles prepared using a conventional method (Chem@AuNPs). (A) Morphologies observed by transmission electron microscopy (top) and the distribution of their diameter (bottom). The diameter of AuNPs was analyzed using ImageJ from measurement of 100 particles in each case. Scale bar, 10 nm. (B) Absorption spectra. (C) Hydrodynamic diameters. (D) Zeta potentials. (E) Fourier transform infrared spectra.

Optimization of AuNP Synthesis. The algal extract/$HAuCl_4$ volume ratio, $HAuCl_4$ concentration, reaction temperature, reaction time, and pH were systematically varied to achieve the desired AuNP size and colloidal stability (Figure 1B,C and Table S2). The formation of AuNPs with the desired diameters of several tens of nanometers was manifested by an absorption peak at ~525 nm, with blue and red shifts indicating smaller- and larger-than-desired diameters, respectively.[36] The optimum algal extract/$HAuCl_4$ ratios were determined as 1:1 and 1:9 for CT@AuNPs and SP@AuNPs, respectively, with the respective absorption peaks appearing at 543 and 535 nm. Despite the absorption peak of SP@AuNPs shifting slightly from 533 nm at a 1:4 algal extract/$HAuCl_4$ volume ratio to 535 nm at 1:9 (Table S2), the latter condition was chosen for the following experiments as it facilitated the completion of the AuNPs synthesis reaction. Increasing the

https://doi.org/10.1021/acssuschemeng.5c07786
ACS Sustainable Chem. Eng. 2025, 13, 19599−19612

Downloaded from http://pubs.acs.org/ascecg/article-pdf/13/45/19599/4245742/sc5c07786.pdf by UNIV OF OSAKA user on 27 July 2026

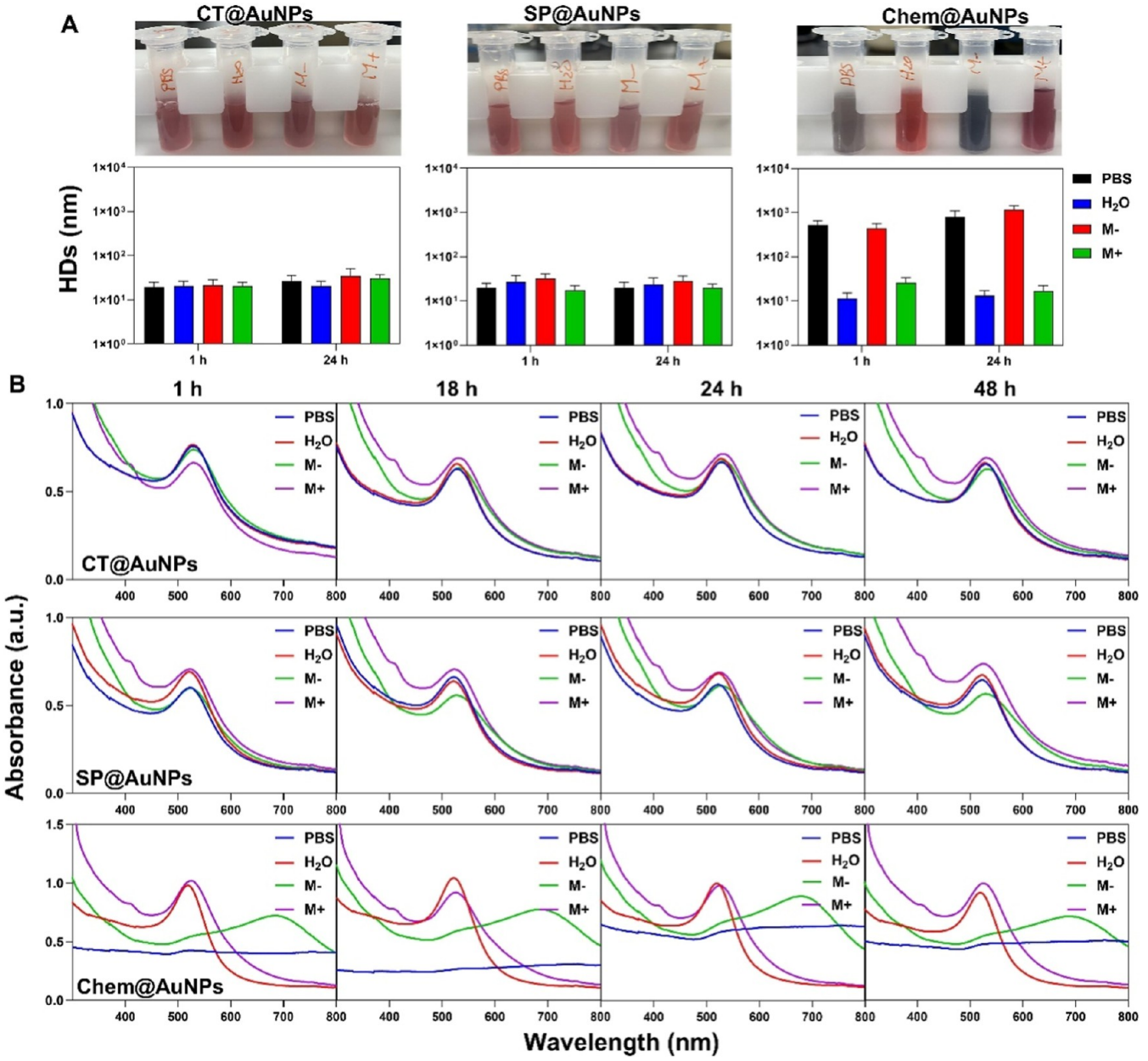


Figure 3. Colloidal stability test of gold nanoparticles (AuNPs). (A) Visual appearances (top) and hydrodynamic diameters (HDs, bottom) of CT@AuNPs, SP@AuNPs, and Chem@AuNPs suspended in water, phosphate-buffered saline (PBS), and phenol red−free Dulbecco's Modified Eagle Medium with (M+) and without (M−) 10% fetal bovine serum and incubated for 1 and 24 h and (B) corresponding absorption spectra recorded at incubation times of 1, 18, 24, and 48 h.

$HAuCl_4$ concentration from 0.5 mM to 1 mM enhanced the formation of larger AuNPs or their agglomeration, as indicated by the red shifts of the corresponding absorption peaks. For both CT@AuNPs and SP@AuNPs, the optimal reaction temperature and time were determined as 95 °C and 15 min, respectively, with the corresponding absorption peaks observed at 543 nm (CT@AuNPs) and 535 nm (SP@AuNPs). Among the tested media (acidic, neutral, and alkaline), that with pH 12 was optimal for producing CT@AuNPs and SP@AuNPs, with the corresponding absorption peaks observed at 528 and 523 nm, respectively (cf. Figure 2B). Deviations from these optimal parameters resulted in no AuNP formation or large/aggregated AuNPs. Finally, the optimum conditions for producing CT@AuNPs and SP@AuNPs with the desired size and stability were determined as algal extract/$HAuCl_4$ ratio = 1:1 (CT@AuNPs) and 1:9 (SP@AuNPs), 0.5 mM $HAuCl_4$, 95 °C, 15 min, and pH 12.

Characterization. The AuNPs produced under the optimal conditions were characterized by TEM, UV−vis spectroscopy, zeta potential measurements, FTIR spectroscopy, and XRD. CT@AuNPs mainly comprised quasispherical particles, although rod-like, triangular, and hexagonal particles were also observed (Figure 2A). The overall average diameter of the CT@AuNP core was determined as 9.5 ± 5.4 nm by examining quasispherical (>100 in number), triangular (4), hexagonal (1), and rod-like (2) particles, with their average diameters equaling 8.8 ± 5.4, 19.6 ± 5.6, 26.51, and 22.9 nm, respectively (Figure 2A). SP@AuNPs and Chem@AuNPs comprised quasispherical particles with average diameters of 5.6 ± 2.2 nm (100 particles) and 11.9 ± 1.7 nm (100

https://doi.org/10.1021/acssuschemeng.5c07786
ACS Sustainable Chem. Eng. 2025, 13, 19599−19612

Downloaded from http://pubs.acs.org/ascecg/article-pdf/13/45/19599/4245742/sc5c07786.pdf by UNIV OF OSAKA user on 27 July 2026

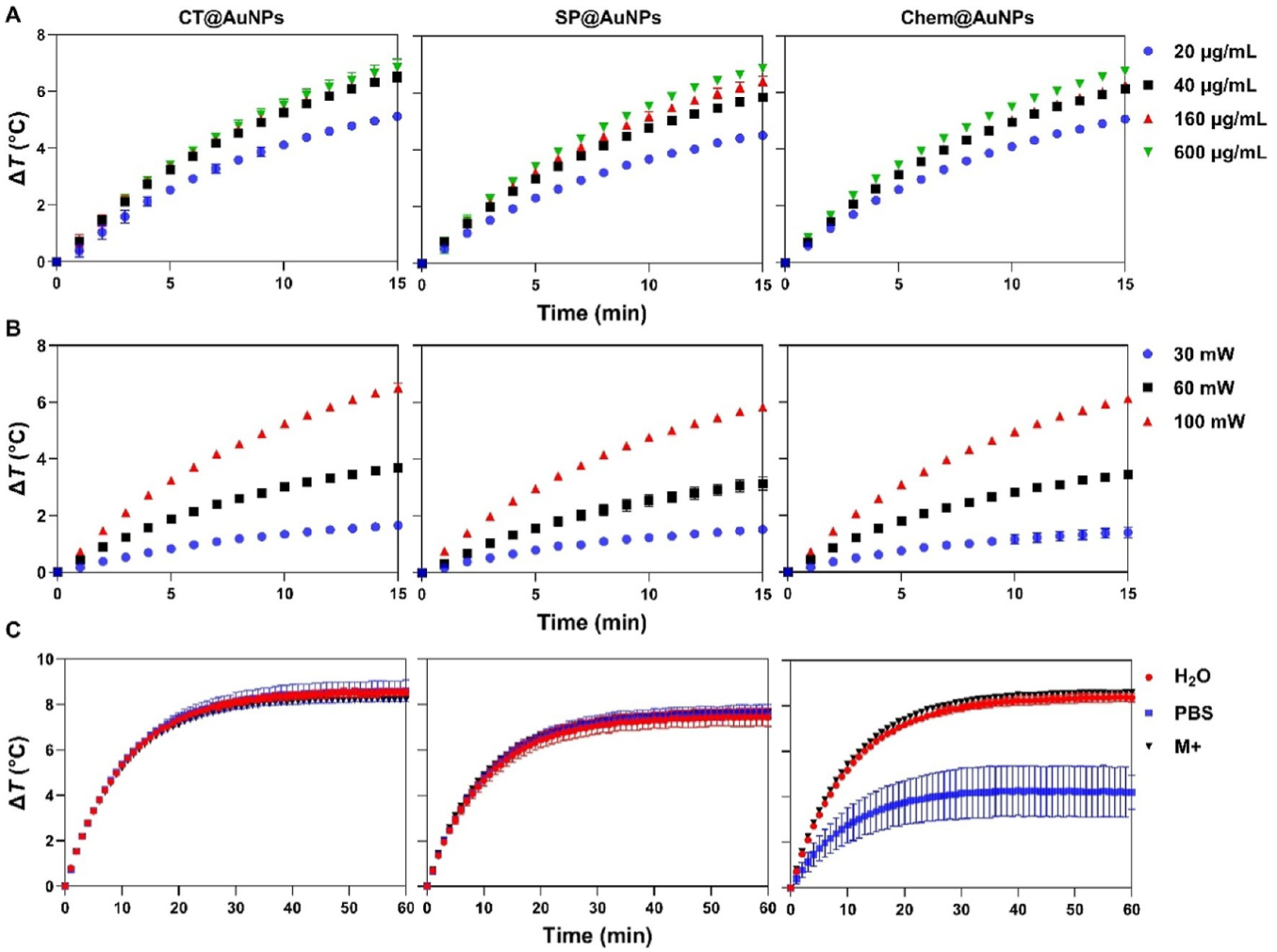


Figure 4. Photothermal behaviors of CT@AuNPs, SP@AuNPs, and Chem@AuNPs. (A) Influence of AuNP concentration and (B) laser power on photothermal activity in water. (C) Photothermal stabilities in water, PBS, and M+ after green laser irradiation for 60 min $n = 3$.

particles), respectively (Figure 2A). CT@AuNPs, SP@AuNPs, and Chem@AuNPs featured absorption peaks at 528, 523, and 519 nm, respectively (Figures 2B and S3), hydrodynamic diameters of 26.8 ± 10.3, 19.2 ± 6.1, and 11.4 ± 3.3 nm, respectively, and polydispersity indices (PDIs) of 0.5, 0.31, and 0.32, respectively (Figures 2C and S4). The PDIs of SP@AuNPs and Chem@AuNPs were lower than that of CT@AuNPs, indicating a more uniform particle size distribution. The moderate PDI of CT@AuNPs was ascribed to the variation in particle shape. CT@AuNPs, SP@AuNPs, and Chem@AuNPs featured zeta potentials of −43.7 ± 5.4, −22.6 ± 11.0 and −30.5 ± 6.9 mV, respectively, i.e., their surfaces were negatively charged (Figure 2D and Figure S4). The XRD patterns of CT@AuNPs and SP@AuNPs exhibited peaks at 2θ = 38.2°, 44.4°, 64.7°, and 77.7°, which were assigned to the 111, 200, 220, and 311 planes of face-centered cubic (FCC) Au (COD 1100138) and indicated the crystalline nature of these NPs (Figure S5). The d-spacings of CT@AuNPs and SP@AuNPs were calculated as 0.23 nm by applying Bragg's law to the peak at 38.2° ($d = \lambda/(2 \sin \theta)$) and corresponded to the spacing between the 111 planes of FCC Au. The existence of algal biomolecules on the surfaces of CT@AuNPs and SP@AuNPs was confirmed using FTIR spectroscopy (Figures 2E and S6−S8), with the main peaks ascribed to the O−H stretching of carbohydrates, C−H stretching of alkyl groups in hydrocarbon segments, C−H bending of alkyl groups in lipids or the aliphatic side chains of proteins and some regions of carbohydrates, C−H bending of alkyl groups in aromatic compounds, C═O stretching, N−H or C−N stretching of proteins, and C−O stretching of lipids, carbohydrates, or proteins. These results suggest that the proteins, polysaccharides, and lipids of *C. thermophila* and *Arthrospira* sp. participated in the synthesis of AuNPs by stabilizing them and acting as reductants.[24,37−39] The FTIR spectrum of Chem@AuNPs, which were synthesized using sodium citrate, featured the strong symmetric and antisymmetric stretching vibrations of citrate COO^- groups at 1395 and 1586 cm^{-1}, respectively. Compared with Chem@AuNPs, which often require multistep synthesis and surface modification, CT@AuNPs and SP@AuNPs provide an alternative with controlled surface functionalities.

Colloidal Stabilities of AuNPs. The stabilities of CT@AuNPs, SP@AuNPs, and Chem@AuNPs were examined in water, PBS, and phenol red−free DMEM with (M+) and without (M−) 10% FBS at 1, 18, 24, and 48 h (Figure 3). CT@AuNP and SP@AuNP suspensions exhibited no visible changes for up to 24 h, in line with the results of dynamic light scattering analysis (Figure 3A). The hydrodynamic diameters of CT@AuNPs and SP@AuNPs exhibited no notable changes with time in all media, in agreement with the corresponding

Downloaded from http://pubs.acs.org/ascecg/article-pdf/13/45/19599/4245742/sc5c07786.pdf by UNIV OF OSAKA user on 27 July 2026

https://doi.org/10.1021/acssuschemeng.5c07786
ACS Sustainable Chem. Eng. 2025, 13, 19599−19612

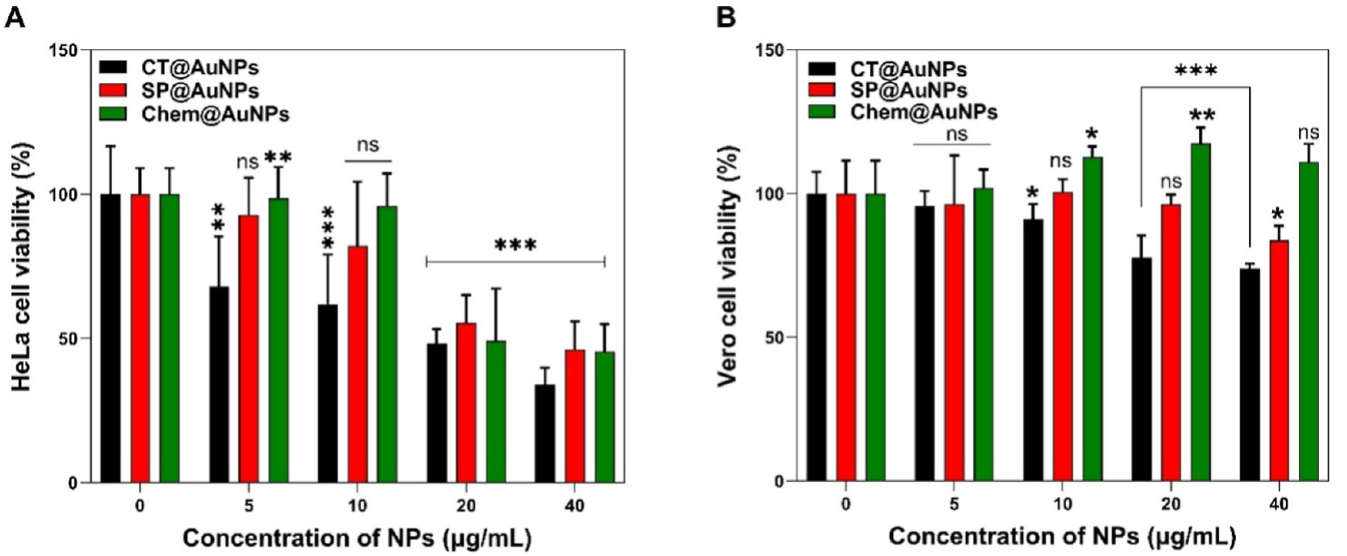


Figure 5. HeLa (A) and Vero (B) cell viabilities after incubation with CT@AuNPs, SP@AuNPs and Chem@AuNPs of various concentrations. Data represent means ± standard deviations (SDs). *p*-values were calculated against untreated cells, with significance thresholds set to ***$p < 0.0001$, **$p < 0.001$, and *$p \leq 0.01$. ns, not significant. The experiments were performed in 6 replicates in HeLa and Vero cells, respectively.

absorption spectra. No notable absorption peak shifts were observed up to 48 h, suggesting colloidal stability in all media (Figure 3B). This finding highlights the role of the algal corona of the AuNPs in preventing their agglomeration. Chem@AuNPs showed colloidal stability only in water and M+, whereas the corresponding suspensions in PBS and M− turned gray, which indicated aggregation, and the hydrodynamic diameter concomitantly increased to 1000 nm (Figure 3A). Furthermore, no characteristic absorption peak at 519 nm was observed for Chem@AuNPs suspended in PBS and M− from the first hour of incubation (Figure 3B), which indicated the instability of Chem@AuNPs in salt-containing solutions.

Photothermal Efficacies and Stabilities of AuNPs. The photothermal efficacies and stabilities of CT@AuNPs, SP@AuNPs, and Chem@AuNPs were examined by measuring the temperature change (ΔT) of their irradiated suspensions in water, PBS, and M+ over time (Figure S9). The ΔT values of CT@AuNP, SP@AuNP, and Chem@AuNP suspensions in water reached 6.5 ± 0.1, 5.8 ± 0.3 and 6.4 ± 0.1 °C, respectively, after 15 min. For CT@AuNP and SP@AuNP suspensions in PBS and M+, ΔT remained unchanged (i.e., equaled that observed for the corresponding suspensions in water), whereas a lower ΔT of 3.4 ± 0.9 °C was observed for Chem@AuNPs in PBS, in line with the poor stability of these NPs in PBS. Water, PBS, and $HAuCl_4$ showed negligible ΔT after 15 min, whereas M+ and *C. thermophila* and *Arthrospira* sp. extracts exhibited ΔT values of 1.6 ± 0.0, 1.7 ± 0.1 and 4.8 ± 0.0 °C, respectively. The photothermal behavior of CT@AuNPs, SP@AuNPs, and Chem@AuNPs was dependent on the NP concentration (Figure 4A) and laser power (Figure 4B). During 1 h of photoexcitation, the ΔT values of CT@AuNPs and SP@AuNPs saturated at approximately 8.6 and 7.6 °C, respectively, in all three solutions, which suggested photothermal stability under these conditions (Figure 4C). On the contrary, for Chem@AuNPs, the saturation ΔT in PBS (4.2 ± 1.0 °C) was substantially lower than the values observed in water (8.4 ± 0.2 °C) and M+ (8.6 ± 0.1 °C). The sustained photothermal effect of Chem@AuNPs in M+ was ascribed to the formation of a protein corona endowing the NPs with stability and dispersibility. Given that protein corona formation corresponds to the nonspecific surface binding of FBS biomolecules by AuNPs, this process is highly dependent on the surface chemistry of the NPs and biomolecules in the serum and poses a risk of unpredictable interactions with and influences on the biological specimens and NP functionality. The large measurement errors observed for Chem@AuNPs in PBS were ascribed to rapid NP aggregation and precipitation. In conclusion, CT@AuNPs and SP@AuNPs exhibited photothermal efficacies similar to but more controllable than that of Chem@AuNPs.

Cytotoxicity of AuNPs. The cytotoxicities of CT@AuNPs, SP@AuNPs, and Chem@AuNPs toward malignant HeLa and nonmalignant Vero cells were examined using the 3-(4,5-dimethylthiazol-2-yl)-2,5-diphenyltetrazolium bromide (MTT) assay (Figure 5). These AuNPs exhibited dose-dependent toxicities toward HeLa cells. At 40 μg/mL CT@AuNPs, SP@AuNPs, and Chem@AuNPs, the viability of HeLa cells decreased to 33.7 ± 6.0%, 46.1 ± 9.7%, and 45.4 ± 9.6%, respectively. In contrast, CT@AuNPs and SP@AuNPs were less toxic toward Vero cells, with the corresponding viabilities at 40 μg/mL equaling 73.9 ± 1.6% and 83.6 ± 5.1%, respectively. Chem@AuNPs had a negligible effect on Vero cell viability at all examined concentrations. Although the biogenic NPs reduced the viability of HeLa cells while demonstrating relatively low toxicities toward Vero cells, obtaining NPs with no toxicity toward normal cells is highly desirable. More studies are required to better understand and mitigate the cytotoxicity of AuNPs.

In Vitro Photothermal Efficacy of AuNPs. The photothermal efficacy of AuNPs was examined in HeLa cells using (i) trypan blue, (ii) intracellular ROS generation, and (iii) morphology assays. (i) The AuNP + laser group showed abundantly distributed blue—stained cells and a cell viability lower than those observed for untreated and AuNP-only groups, which indicated that the AuNP-induced photothermal effect contributed to cell killing (Figure 6A). After 24 h, treatment with CT@AuNPs, SP@AuNPs, and Chem@AuNPs reduced a HeLa cell viability to ∼70%, whereas the same treatment combined with laser stimulation led to a reduced viability of ∼30%, which indicated that the photothermal effect

Downloaded from http://pubs.acs.org/ascecg/article-pdf/13/45/19599/4245742/sc5c07786.pdf by UNIV OF OSAKA user on 27 July 2026

https://doi.org/10.1021/acssuschemeng.5c07786
ACS Sustainable Chem. Eng. 2025, 13, 19599−19612

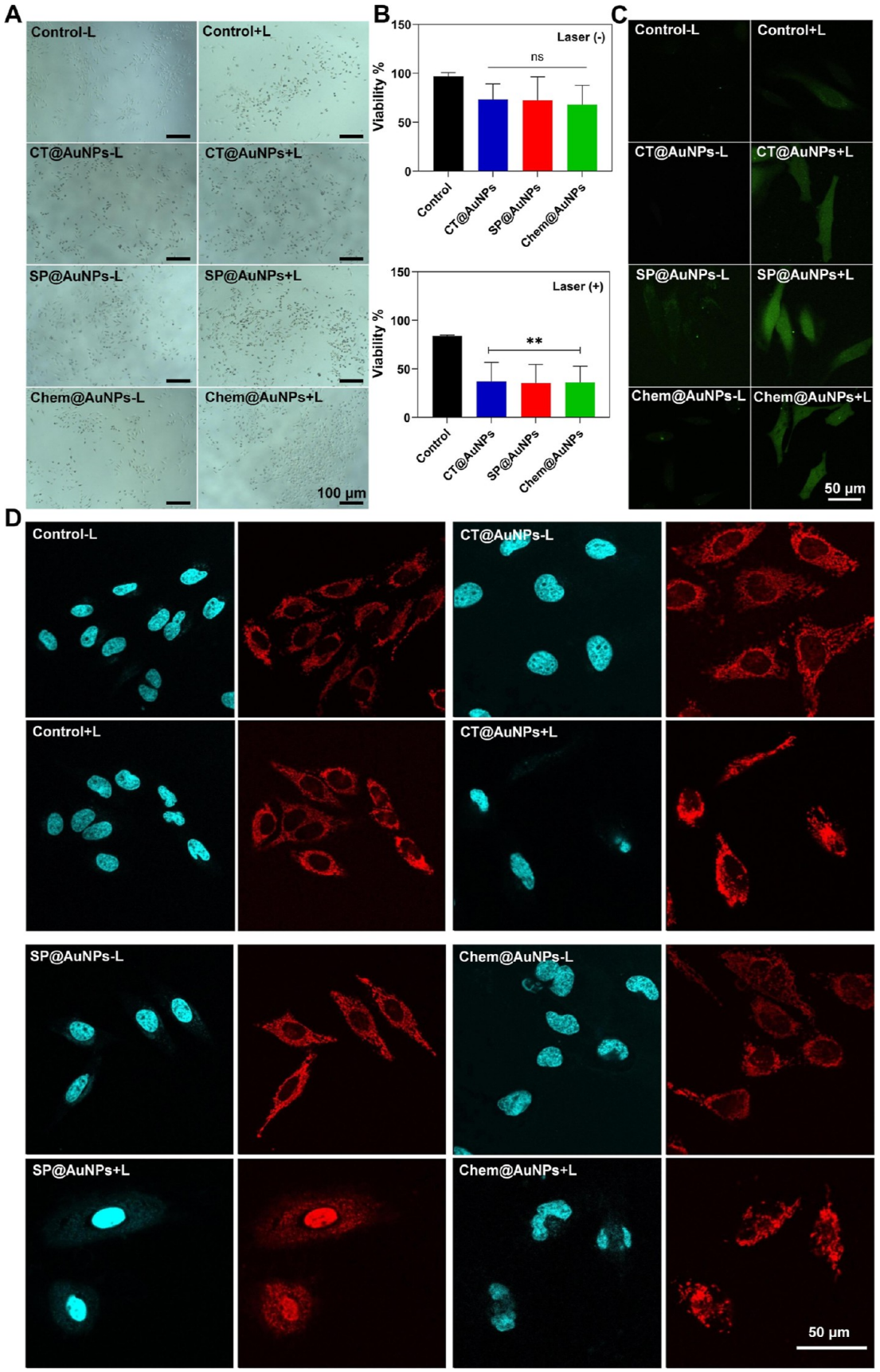


Figure 6. Anticancer efficacies of AuNPs under laser irradiation. (A) Inverted light microscopy images of trypan blue—stained HeLa cells before (−L) and after (+L) laser irradiation at 24 h. Scale bar, 100 μm. (B) Viabilities of HeLa cells before (top) and after (bottom) photoexcitation were assessed by cell counting and the trypan blue assay at 24 h. Data are presented as means ± SDs. p-values were calculated against untreated cells, with the significance threshold set to $^{**}p < 0.001$. ns; not significant. The experiments were performed in 3 replicates. (C) Intracellular ROS

https://doi.org/10.1021/acssuschemeng.5c07786
ACS Sustainable Chem. Eng. 2025, 13, 19599−19612

Downloaded from http://pubs.acs.org/ascecg/article-pdf/13/45/19599/4245742/sc5c07786.pdf by UNIV OF OSAKA user on 27 July 2026

Figure 6. continued

generation in HeLa cells after photoexcitation at 24 h were estimated using the 2′,7′-dichlorofluorescein assay. Scale bar, 50 μm. (D) Confocal fluorescence microscopy images of HeLa cells stained with Hoechst (cyan) and MitoTracker Red (red). Scale bar, 50 μm. See Figures S10−S13 for expanded images.

of these AuNPs increased their toxicity (Figure 6B). (ii) Cellular damage due to AuNP-associated photothermal effect may be caused by the overproduction of ROS upon photoexcitation (the currently proposed mechanism is described in the next paragraph).[33,34] We examined the intracellular ROS in all tested groups using a DCFH-DA (Figure 6C). Mechanistically, dichlorodihydrofluorescein is oxidized by ROS and transformed to dichlorofluorescein, which produces green fluorescence (excitation/emission peaks at 485/530 nm).[40] Weak green fluorescence was recorded in cells treated with CT@AuNPs, SP@AuNPs, and Chem@AuNPs (cf. absence of fluorescence in untreated cells), indicating a low amount of ROS generation. On the contrary, strong green fluorescence was observed when the AuNP treatment was combined with laser irradiation, corresponding to a notable increase in ROS generation compared to the laser-only treatment. (iii) In the morphology assay, the cells were treated with CT@AuNPs, SP@AuNPs, and Chem@AuNPs for 3 h and stimulated with a green laser, and the nuclei and mitochondria were subsequently stained with Hoechst and MitoTracker Red fluorescent dyes, respectively (Figures 6D and S10−S13). Live-cell confocal fluorescence micrographs showed that in the absence of the AuNPs, both nontreated and laser-stimulated cells had intact nuclei and fibrous morphologies characteristic of healthy mitochondria. Only a few cells treated with CT@AuNPs, SP@AuNPs, and Chem@AuNPs exhibited chromatin condensation and fragmented punctate structures of mitochondria (both of which are indicators of apoptosis) instead of the thread-like morphology.[33,41] However, laser irradiation in the presence of the AuNPs damaged the cells and the morphological changes observed for CT@AuNPs and SP@AuNPs were more severe than those observed for Chem@AuNPs. Previous works demonstrated that ROS generated upon photoexcitation induce intensive oxidative stress by interacting with cellular biomolecules, interfering with antioxidant defenses, and damaging proteins and DNA, thus inflicting substantial cellular damage.[33,34,42] Thus, the HeLa cell damage observed after photoexcitation was tentatively ascribed to the combination of photoinduced oxidative stress and heat stress—mediated toxicity,[33,41] supporting the role of AuNPs as photothermal agents and photosensitizers mediating ROS generation.

DISCUSSION

Unlike conventional routes, the green synthesis of NPs using biological agents such as microalgae, plants, and fungi offers particular advantages in biocompatibility and stability. Among those, microalgae are photosynthetic organisms that are rich in nutrients, biomolecules, and metabolites, and they exhibit the ability to detoxify heavy metals. These features make them promising candidates for NP synthesis.[18,43] In this study, we presented a microalgae-mediated method for synthesizing AuNPs with colloidal and photothermal stability. This one-pot process, when the conditions were optimized, yielded small (<25 nm) and surface-functionalized AuNPs without additional toxic chemicals (Figures 1 and 2), addressing a persistent challenge of multistep chemical synthesis processes. The use of microalgae avoided the need for additional surfactants and reduced the use or generation of toxic substances, thus contributing to an eco-friendly alternative. Our data indicate that these advantages stem from a set of biomolecules in the algal extract (Figures 2 and S6−S8, and Table S1), which act as a biomachinery for NP synthesis by providing reduction and stabilization potentials, as previously demonstrated.[17,44,45]

We isolated a novel microalgal strain morphologically and genetically identified as 96.66% similar to the *C. thermophila* var. *globulina* isolate FACHB-2308. The morphologies of this strain and *Arthrospira* sp. agreed with those reported by Boutarfa et al. and Wang and Zhao, respectively.[25,46] To the best of our knowledge, our study is the first-time account of the potential of this new strain to reduce $HAuCl_4$ and stabilize the resulting AuNPs, providing a detailed analysis of the AuNP shape, size, and other properties. *Arthrospira* sp. was selected as an FDA-approved cyanobacterium with a known reducing potential for synthesizing AuNPs.[28,47] Unfortunately, very few previous reports before the current study have relied on reaction parameter control to obtain AuNPs with the desirable size and stability for photothermal applications.

The high sensitivity of CT@AuNP and SP@AuNP properties to reaction parameters indicates the importance of kinetic control in green synthesis (Figure 1C). Higher concentrations or imbalanced reductant/$HAuCl_4$ ratios resulted in the formation of larger AuNPs or aggregates, possibly because the AuNP size and stability depended on the reactant concentration, which was directly correlated with the availability of reductants and Au^{3+} ions for reduction.[48] High $HAuCl_4$ concentrations favor the formation of large AuNPs, probably because of the increased amount of Au^{3+} ions available for nucleation and growth under these conditions.[49,50] Moreover, the reaction temperature and time substantially affect the synthesis of AuNPs by influencing their nucleation and growth rates and, hence, their morphology, dispersibility, and stability.[51,52] The conditions of CT@AuNP and SP@AuNP syntheses favored thermodynamic growth at short reaction times. We propose that thermally activated reducing agents (algal biomolecules) increase the reaction rate and thus favor rapid nucleation rather than prolonged growth, preventing the formation of larger NPs.[51] Consistently, exposure to high temperatures for >15 min led to the conversion of more Au^{3+} into AuNPs or/and biomolecule degradation/denaturation, thus causing the formation of large NPs or aggregates.[48,53,54] Our data show that the size of AuNPs varied considerably with pH. Smaller and more uniform AuNPs were produced at an alkaline pH, whereas larger AuNPs were observed at neutral and acidic pH levels. This variation can be attributed to the composition of metabolites that determines pH sensitivity and influences the aggregation dynamics of AuNPs. The charge states of functional groups such as hydroxyl, carboxyl, amide, and thiol in polysaccharides, phenols, and proteins are pH-dependent, which in turn regulates their electron-donating capacity for Au^{3+} reduction. At pH > 7, deprotonation increases the reactivity of these groups and enhances electron

Downloaded from http://pubs.acs.org/ascecg/article-pdf/13/45/19599/4245742/sc5c07786.pdf by UNIV OF OSAKA user on 27 July 2026

https://doi.org/10.1021/acssuschemeng.5c07786
ACS Sustainable Chem. Eng. 2025, 13, 19599−19612

transfer from reductants. This accelerates the reduction of Au^{3+} to Au^0 and promotes rapid nucleation, resulting in smaller and more uniform AuNPs. At pH 12, further ionization of algal functional groups such as COO^- and OH^- enhances their ability to cap the resultant AuNPs and increases the electrostatic repulsion, thereby reducing aggregation.[55,56] In contrast, under acidic pH, limited deprotonation slows the reduction kinetics and decreases electrostatic stabilization, which promotes the growth and aggregation of large AuNPs. These findings are consistent with previous reports showing that alkaline pH favors the formation of small AuNPs.[56−58]

Although the exact mechanism of AuNP synthesis by microalgae remains under investigation, previous studies suggest that it is mediated by the redox activity of algal metabolites, which act as both reducing and stabilizing agents.[59] Algal extracts contain biomolecules such as phenols, flavonoids, proteins, and polysaccharides, which exhibit radical scavenging activity.[60−63] The redox potential of these biomolecules enables them to donate electrons to Au^{3+} ions, reducing them to the atomic state (Au^0) and thereby initiating nucleation and growth. Subsequently, proteins, polysaccharides, and lipids coat the surface of AuNPs, providing steric and electrostatic stabilization (Figure 1B). Algae can accumulate large quantities of fatty acids and therefore survive in harsh environments. These fatty acids make microalgae promising candidates for biotechnology applications.[17,25,64,65] Our data highlight the importance of the *C. thermophila* var. *globulina* isolate FACHB-2308 as a novel enriched source of fatty acids. *C. thermophila* and *Arthrospira* sp. extracts had remarkable fatty acid profiles (Figures 2E and S2). These results are consistent with previous studies in which the *C. thermophila* var. *globulina* strain was demonstrated to have high contents of oleic acid (35.95 ± 0.07%), palmitic acid (21.45 ± 0.12%), and linoleic acid (14.38 ± 0.03%),[25] whereas *Arthrospira* sp. was shown to contain linoleic acid methyl ester (30.3%), palmitic acid methyl ester (29.69%), and oleic acid methyl ester (20.22%).[66] Lipids act as a protective NP coating, preventing aggregation because of their amphiphilic properties, with their hydrophobic hydrocarbon chains covering the NP surface while hydrophilic carboxylate groups interacting with the aqueous environment.[67] Several studies used fatty acids, namely palmitic,[68] oleic,[69] and linoleic[70] acids, as capping agents for NP preparation. Thus, the fatty acids identified in *C. thermophila* and *Arthrospira* sp. could be the main stabilizing agents during the synthesis of CT@AuNPs and SP@AuNPs.

The current study successfully demonstrates another benefit of algal biomolecules. The stability of NPs after prolonged irradiation is a crucial factor that determines PTT performance, enabling consistent heat release upon photoexcitation without NP aggregation or loss of efficacy.[71] Compared with Chem@AuNPs, CT@AuNPs and SP@AuNPs provide viable alternatives with inherent surface functionalities enhancing their photothermal performance and stability in various media (Figure 4). The adsorption of algal proteins, polysaccharides, and lipids on the CT@AuNP and SP@AuNP surfaces is considered the main origin of their enhanced interfacial and optical properties and reduced agglomeration propensity. The variation in the toxicities of the AuNPs toward HeLa and Vero cells (Figure 5) is ascribed to that in the AuNP surface chemistry, which facilitates the interaction of the AuNPs with the cell plasma membrane and thus affects NP internalization and oxidative stress generation in cells.[15] Our results also suggest that a hybrid approach, in which chemically synthesized AuNPs are subsequently coated with algal extracts, could be a promising alternative to combine size homogeneity with enhanced biocompatibility.

CONCLUSIONS

The low colloidal stability of AuNPs prepared using conventional methods hinders their biomedical and industrial applications. Our study describes a facile and sustainable green synthesis of surface-functionalized AuNPs that have sizes of several tens of nanometers and are colloidally stable in photothermal applications in the absence of additional surfactants. The functionalized surface of the AuNPs resulted in their enhanced colloidal stability and, hence, improved photothermal properties. Compared with Chem@AuNPs, CT@AuNPs and SP@AuNPs exhibited higher colloidal and photothermal stabilities and photothermal performances under green laser irradiation. Furthermore, owing to the synergy between thermal stress and ROS generation, CT@AuNPs and SP@AuNPs effectively eradicated HeLa cells upon photoexcitation, as demonstrated by nucleus fragmentation, chromatin condensation, and mitochondrial dysfunction (Figures 6C,D, and S10−S13). Although we successfully synthesized CT@AuNPs and SP@AuNPs using microalgae, the precise synthesis mechanism and the identity of the metabolites responsible for AuNP formation remain unclear. Further metabolomic and proteomic studies are required to elucidate the underlying mechanism. In addition, strategies to tune the LSPR of AuNPs into the near-infrared region by modulating particle size and shape will be needed to improve tissue penetration and enhance their effectiveness in in vivo photothermal therapy. Overall, the green synthesis of AuNPs paves the way for the use of biogenic NPs in numerous biomedical applications, such as drug delivery, bioimaging, biosensing, and catalysis, and highlights the unexplored potential of these NPs due to their sustainable, simple, and inexpensive synthesis and high colloidal stability.

ASSOCIATED CONTENT

Data Availability Statement

All data necessary to support the conclusions of this study are included within the paper and its Supporting Information. Additional data sets related to this research are available from the corresponding author upon reasonable request.

Supporting Information

The Supporting Information is available free of charge at https://pubs.acs.org/doi/10.1021/acssuschemeng.5c07786.

Detailed description of the FTIR spectra of CT@AuNPs and SP@AuNPs; phylogenetic tree of the *C. thermophila* var. *globulina* isolate FACHB-2308; GC−MS profiles of *C. thermophila* and *Arthrospira* sp. aqueous extracts; absorption spectra of *C. thermophila* and *Arthrospira* sp., $HAuCl_4$ solution, CT@AuNPs, SP@AuNPs, and Chem@AuNPs; hydrodynamic diameters and zeta potentials of CT@AuNPs, SP@AuNPs, and Chem@AuNPs; XRD patterns of CT@AuNPs and SP@AuNPs; FTIR spectra of CT@AuNPs and SP@AuNPs; temperature profiles of water, PBS, M−, M+, algal extracts, and AuNP dispersions; confocal fluorescence microscopy images of HeLa cells treated with CT@AuNPs, SP@AuNPs and Chem@AuNPs before and after exposure to the green laser; table of volatiles detected in the aqueous extracts of *C. thermophila* and *Arthrospira* sp.; table of

Downloaded from http://pubs.acs.org/ascecg/article-pdf/13/45/19599/4245742/sc5c07786.pdf by UNIV OF OSAKA user on 27 July 2026

https://doi.org/10.1021/acssuschemeng.5c07786
ACS Sustainable Chem. Eng. 2025, 13, 19599−19612

physicochemical properties of CT@AuNPs, SP@AuNPs and Chem@AuNPs (PDF)

AUTHOR INFORMATION

Corresponding Author

Madoka Suzuki − *Institute for Protein Research, The University of Osaka, Osaka 565-0871, Japan;* orcid.org/0000-0002-3270-1755; Email: suzu_mado@protein.osaka-u.ac.jp

Authors

Reham Samir Hamida − *Department of Biological Sciences, Graduate School of Science, The University of Osaka, Osaka 560-0043, Japan; Institute for Protein Research, The University of Osaka, Osaka 565-0871, Japan;* orcid.org/0000-0003-2441-6599

Shingo Sotoma − *Faculty of Molecular Chemistry and Engineering, Kyoto Institute of Technology, Kyoto 606-8585, Japan*

James Chen Yong Kah − *Department of Biomedical Engineering, National University of Singapore, Singapore 117583, Singapore;* orcid.org/0000-0002-2247-6929

Yoshie Harada − *Institute for Protein Research and Premium Research Institute for Human Metaverse Medicine (WPI-PRIMe), The University of Osaka, Osaka 565-0871, Japan; Center for Quantum Information and Quantum Biology, The University of Osaka, Osaka 560-0043, Japan*

Complete contact information is available at: https://pubs.acs.org/10.1021/acssuschemeng.5c07786

Author Contributions

R.S.H., S.S., Y.H., and M.S. designed the experiments. R.S.H. conducted the experiments and analyzed the data. R.S.H. and M.S. visualized the data and drafted the manuscript. R.S.H., S.S., J.K., Y.H., and M.S. revised and corrected the manuscript. All authors have reviewed and approved the final version of the manuscript.

Notes

The authors declare no competing financial interest.

ACKNOWLEDGMENTS

The authors gratefully acknowledge Professor Mashael Mohammed Bin-Meferij, Princess Nourah bint Abdulrahman University, Riyadh, Saudi Arabia for providing the laboratory facilities and technical support required for the isolation of algal strains utilized in this study. This work was supported by JSPS KAKENHI (Grant Numbers 24H02306 to Y.H., and 22H05053 and 25K02242 to M.S.), MEXT Q-LEAP (JPMXS0120330644 to Y.H.), JST CREST (JPMJCR24B6 to Y.H.), JSPS Bilateral Program Number JPJSBP120255707 (to M.S.), and Takeda Science Foundation (to M.S.).

ABBREVIATIONS

AuNPs, gold nanoparticles; Chem@AuNPs, gold nanoparticles prepared using a conventional method; CT@AuNPs, gold nanoparticles prepared using *Coelastrella thermophila* extract; LSPR, localized surface plasmon resonance; DCFH-DA, 2′,7′-dichlorodihydrofluorescein diacetate; DMEM, Dulbecco's Modified Eagle Medium; FBS, fetal bovine serum; FCC, face-centered cubic; FTIR, Fourier transform infrared; GC-MS, gas chromatography−mass spectrometry; M+, Dulbecco's Modified Eagle Medium with 10% fetal bovine serum; M−, Dulbecco's Modified Eagle Medium without 10% fetal bovine serum; NP, nanoparticle; PBS, phosphate-buffered saline; PDI, polydispersity index; PTT, photothermal therapy; ROS, reactive oxygen species; SD, standard deviation; SP@AuNPs, gold nanoparticles prepared using *Arthrospira* sp. extract; TEM, transmission electron microscopy; UV−vis, ultraviolet−visible; XRD, X-ray diffraction

REFERENCES

(1) Ngernpimai, S.; Puangmali, T.; Kopwitthaya, A.; Tippayawat, P.; Chompoosor, A.; Teerasong, S. Enhanced Stability of Gold Nanoparticles with Thioalkylated Carboxyl-Terminated Ligands for Applications in Biosensing. *ACS Appl. Nano Mater.* **2024**, *7* (11), 13124−13133.

(2) Fergusson, J.; Wallace, G. Q.; Sloan-Dennison, S.; Carland, R.; Shand, N. C.; Graham, D.; Faulds, K. Plasmonic and photothermal properties of silica-capped gold nanoparticle aggregates. *J. Phys. Chem. C* **2023**, *127* (50), 24475−24486.

(3) Bansal, S. A.; Kumar, V.; Karimi, J.; Singh, A. P.; Kumar, S. Role of gold nanoparticles in advanced biomedical applications. *Nanoscale Adv.* **2020**, *2* (9), 3764−3787.

(4) Marino, A.; Arai, S.; Hou, Y.; Degl'Innocenti, A.; Cappello, V.; Mazzolai, B.; Chang, Y.-T.; Mattoli, V.; Suzuki, M.; Ciofani, G. Gold nanoshell-mediated remote myotube activation. *ACS Nano* **2017**, *11* (3), 2494−2508.

(5) Ranjana, R.; Parushuram, N.; Harisha, K.; Narayana, B.; Sangappa, Y. Photo-driven synthesis of anisotropic gold nanoparticles using silk fibroin—cell viability activities in lymphocyte and Jurkat cancer cells. *BioNanoScience* **2020**, *10* (4), 864−875.

(6) Uusitalo, M.; Strach, M.; Eriksson, G.; Dmytrenko, T.; Andersson, J.; Dahlin, A.; Hulander, M.; Andersson, M. Photothermal Properties of Solid-Supported Gold Nanorods. *Nano Lett.* **2024**, *24* (40), 12529−12535.

(7) Moustaoui, H.; Saber, J.; Djeddi, I.; Liu, Q.; Diallo, A. T.; Spadavecchia, J.; Lamy de la Chapelle, M.; Djaker, N. Shape and size effect on photothermal heat elevation of gold nanoparticles: absorption coefficient experimental measurement of spherical and urchin-shaped gold nanoparticles. *J. Phys. Chem. C* **2019**, *123* (28), 17548−17554.

(8) Qin, Z.; Bischof, J. C. Thermophysical and biological responses of gold nanoparticle laser heating. *Chem. Soc. Rev.* **2012**, *41* (3), 1191−1217.

(9) Huang, X.; Jain, P. K.; El-Sayed, I. H.; El-Sayed, M. A. Plasmonic photothermal therapy (PPTT) using gold nanoparticles. *Laser Med. Sci.* **2008**, *23*, 217−228.

(10) Mocan, L.; Ilie, I.; Tabaran, F. A.; Dana, B.; Zaharie, F.; Zdrehus, C.; Puia, C.; Mocan, T.; Muntean, V.; Teodora, P.; et al. Surface plasmon resonance-induced photoactivation of gold nanoparticles as mitochondria-targeted therapeutic agents for pancreatic cancer. *Expert Opin. Ther. Targets* **2013**, *17* (12), 1383−1393.

(11) Fazal, S.; Jayasree, A.; Sasidharan, S.; Koyakutty, M.; Nair, S. V.; Menon, D. Green synthesis of anisotropic gold nanoparticles for photothermal therapy of cancer. *ACS Appl. Mater. Interfaces* **2014**, *6* (11), 8080−8089.

(12) Melancon, M. P.; Lu, W.; Zhong, M.; Zhou, M.; Liang, G.; Elliott, A. M.; Hazle, J. D.; Myers, J. N.; Li, C.; Stafford, R. J. Targeted multifunctional gold-based nanoshells for magnetic resonance-guided laser ablation of head and neck cancer. *Biomaterials* **2011**, *32* (30), 7600−7608.

(13) Gao, J.; Huang, X.; Liu, H.; Zan, F.; Ren, J. Colloidal stability of gold nanoparticles modified with thiol compounds: bioconjugation and application in cancer cell imaging. *Langmuir* **2012**, *28* (9), 4464−4471.

(14) Sotoma, S.; Harada, Y. Polydopamine coating as a scaffold for ring-opening chemistry to functionalize gold nanoparticles. *Langmuir* **2019**, *35* (25), 8357−8362.

Downloaded from http://pubs.acs.org/ascecg/article-pdf/13/45/19599/4245742/sc5c07786.pdf by UNIV OF OSAKA user on 27 July 2026

(15) Carnovale, C.; Bryant, G.; Shukla, R.; Bansal, V. Identifying trends in gold nanoparticle toxicity and uptake: size, shape, capping ligand, and biological corona. *ACS Omega* **2019**, *4* (1), 242−256.
(16) Xu, L.; Zhu, Z.; Sun, D.-W. Bioinspired nanomodification strategies: moving from chemical-based agrosystems to sustainable agriculture. *ACS Nano* **2021**, *15* (8), 12655−12686.
(17) Arteaga-Castrejón, A. A.; Agarwal, V.; Khandual, S. Microalgae as a potential natural source for the green synthesis of nanoparticles. *Chem. Commun.* **2024**, *60*, 3874−3890.
(18) Chan, S. S.; Low, S. S.; Chew, K. W.; Ling, T. C.; Rinklebe, J.; Juan, J. C.; Ng, E. P.; Show, P. L. Prospects and environmental sustainability of phyconanotechnology: A review on algae-mediated metal nanoparticles synthesis and mechanism. *Environ. Res.* **2022**, *212*, 113140.
(19) Shang, H.; Ma, C.; Li, C.; Cai, Z.; Shen, Y.; Han, L.; Wang, C.; Tran, J.; Elmer, W. H.; White, J. C.; et al. Aloe vera extract gel-biosynthesized selenium nanoparticles enhance disease resistance in lettuce by modulating the metabolite profile and bacterial endophytes composition. *ACS Nano* **2023**, *17* (14), 13672−13684.
(20) Li, X.; Mao, X.; Xie, W.; Liu, B.; Chen, F. Intracellular biosynthesis of gold nanoparticles for monitoring microalgal biomass via surface-enhanced Raman spectroscopy. *ACS Sustainable Chem. Eng.* **2022**, *10* (15), 4872−4880.
(21) Chellapandian, C.; Ramkumar, B.; Puja, P.; Shanmuganathan, R.; Pugazhendhi, A.; Kumar, P. Gold nanoparticles using red seaweed Gracilaria verrucosa: Green synthesis, characterization and biocompatibility studies. *Process Biochem.* **2019**, *80*, 58−63.
(22) Dahoumane, S. A.; Mechouet, M.; Wijesekera, K.; Filipe, C. D.; Sicard, C.; Bazylinski, D. A.; Jeffryes, C. Algae-mediated biosynthesis of inorganic nanomaterials as a promising route in nanobiotechnology−a review. *Green Chem.* **2017**, *19* (3), 552−587.
(23) MubarakAli, D.; Arunkumar, J.; Nag, K. H.; SheikSyedIshack, K.; Baldev, E.; Pandiaraj, D.; Thajuddin, N. Gold nanoparticles from Pro and eukaryotic photosynthetic microorganisms—Comparative studies on synthesis and its application on biolabelling. *Colloids Surf., B* **2013**, *103*, 166−173.
(24) Zayadi, R. A.; Bakar, F. A. Comparative study on stability, antioxidant and catalytic activities of bio-stabilized colloidal gold nanoparticles using microalgae and cyanobacteria. *J. Environ. Chem. Eng.* **2020**, *8* (4), 103843.
(25) Boutarfa, S.; Senoussi, M. M.; Gonzalez-Silvera, D.; López-Jiménez, J. Á.; Aboal, M. The Green Microalga Coelastrella thermophila var. globulina (Scenedesmaceae, Chlorophyta) isolated from an Algerian hot spring as a potential source of fatty acids. *Life* **2022**, *12* (4), 560.
(26) Hamida, R. S.; Ali, M. A.; Almohawes, Z. N.; Alahdal, H.; Momenah, M. A.; Bin-Meferij, M. M. Green synthesis of hexagonal silver nanoparticles using a novel microalgae coelastrella aeroterrestrica strain BA_Chlo4 and resulting anticancer, antibacterial, and antioxidant activities. *Pharmaceutics* **2022**, *14* (10), 2002.
(27) Liang, F.; Zheng, Y.; Zhao, C.; Li, L.; Hu, Y.; Wang, C.; Wang, R.; Feng, T.; Liu, X.; Cui, J.; et al. Microalgae-derived extracellular vesicles synergize with herbal hydrogel for energy homeostasis in osteoarthritis treatment. *ACS Nano* **2025**, *19* (8), 8040−8057.
(28) Huang, G.; Chen, X.; Li, N.; Xie, T.; Guo, Y.; Fu, Y.; Jiao, T. A convenient synthesis of gold nanoparticles in Spirulina extract for rapid visual detection of dopamine in human urine. *Colloids Surf., A* **2022**, *650*, 129675.
(29) Bolch, C. J.; Orr, P. T.; Jones, G. J.; Blackburn, S. I. Genetic, morphological, and toxicological variation among globally distributed strains of Nodularia (Cyanobacteria). *J. Phycol.* **1999**, *35* (2), 339−355.
(30) Khaw, Y. S.; Khong, N. M. H.; Shaharuddin, N. A.; Yusoff, F. M. A simple 18S rDNA approach for the identification of cultured eukaryotic microalgae with an emphasis on primers. *J. Microbiol. Methods* **2020**, *172*, 105890.
(31) Hamida, R. S.; Ali, M. A.; Mugren, N.; Al-Zaban, M. I.; Bin-Meferij, M. M.; Redhwan, A. Planophila laetevirens-Mediated Synthesis of Silver Nanoparticles: optimization, Characterization, and Anticancer and Antibacterial Potentials. *ACS Omega* **2023**, *8* (32), 29169−29188.
(32) Mosmann, T. Rapid colorimetric assay for cellular growth and survival: application to proliferation and cytotoxicity assays. *J. Immunol. Methods* **1983**, *65* (1−2), 55−63.
(33) Guerrero-Florez, V.; Mendez-Sanchez, S. C.; Patrón-Soberano, O. A.; Rodríguez-González, V.; Blach, D.; Martínez, O. F. Gold nanoparticle-mediated generation of reactive oxygen species during plasmonic photothermal therapy: a comparative study for different particle sizes, shapes, and surface conjugations. *J. Mater. Chem. B* **2020**, *8* (14), 2862−2875.
(34) Broadbent, M.; Chadwick, S. J.; Brust, M.; Volk, M. Gold Nanoparticles for Photothermal and Photodynamic Therapy. *ACS Omega* **2024**, *9* (44), 44846−44859.
(35) Tian, Y.; Nusantara, A. C.; Hamoh, T.; Mzyk, A.; Tian, X.; Perona Martinez, F.; Li, R.; Permentier, H. P.; Schirhagl, R. Functionalized fluorescent nanodiamonds for simultaneous drug delivery and quantum sensing in HeLa cells. *ACS Appl. Mater. Interfaces* **2022**, *14* (34), 39265−39273.
(36) He, Y. Q.; Liu, S. P.; Kong, L.; Liu, Z. F. A study on the sizes and concentrations of gold nanoparticles by spectra of absorption, resonance Rayleigh scattering and resonance non-linear scattering. *Spectrochim. Acta, Part A* **2005**, *61* (13−14), 2861−2866.
(37) Suganya, K. U.; Govindaraju, K.; Kumar, V. G.; Dhas, T. S.; Karthick, V.; Singaravelu, G.; Elanchezhiyan, M. Blue green alga mediated synthesis of gold nanoparticles and its antibacterial efficacy against Gram positive organisms. *Mater. Sci. Eng., C* **2015**, *47*, 351−356.
(38) Gallón, S. M. N.; Alpaslan, E.; Wang, M.; Larese-Casanova, P.; Londoño, M. E.; Atehortúa, L.; Pavón, J. J.; Webster, T. J. Characterization and study of the antibacterial mechanisms of silver nanoparticles prepared with microalgal exopolysaccharides. *Mater. Sci. Eng., C* **2019**, *99*, 685−695.
(39) Yue, Y.; Yokota, Y.; Uchihashi, T. Biosynthesis of highly branched gold nanoparticles through structural engineering of fatty acids. *iScience* **2023**, *26* (1), 105864.
(40) Kim, H.; Xue, X. Detection of total reactive oxygen species in adherent cells by 2', 7'-dichlorodihydrofluorescein diacetate staining. *J. Visualized Exp.* **2020**, *160*, No. e60682.
(41) Bajpai, A.; Desai, N. N.; Pandey, S.; Shukla, C.; Datta, B.; Basu, S. Chimeric nanoparticles for targeting mitochondria in cancer cells. *Nanoscale Adv.* **2022**, *4* (4), 1112−1118.
(42) Kessler, A.; Hedberg, J.; Blomberg, E.; Odnevall, I. Reactive oxygen species formed by metal and metal oxide nanoparticles in physiological media—a review of reactions of importance to nanotoxicity and proposal for categorization. *Nanomaterials* **2022**, *12* (11), 1922.
(43) Jacob, J. M.; Ravindran, R.; Narayanan, M.; Samuel, S. M.; Pugazhendhi, A.; Kumar, G. Microalgae: A prospective low cost green alternative for nanoparticle synthesis. *Curr. Opin. Environ. Sci. Health* **2021**, *20*, 100163.
(44) Koul, B.; Poonia, A. K.; Yadav, D.; Jin, J.-O. Microbe-mediated biosynthesis of nanoparticles: Applications and future prospects. *Biomolecules* **2021**, *11* (6), 886.
(45) Chopra, H.; Bibi, S.; Singh, I.; Hasan, M. M.; Khan, M. S.; Yousafi, Q.; Baig, A. A.; Rahman, M. M.; Islam, F.; Emran, T. B.; et al. Green metallic nanoparticles: biosynthesis to applications. *Front. Bioeng. Biotechnol.* **2022**, *10*, 874742.
(46) Wang, Z. P.; Zhao, Y. Morphological reversion of Spirulina (Arthrospira) platensis (Cyanophyta): from linear to helical 1. *J. Phycol.* **2005**, *41* (3), 622−628.
(47) Dananjaya, S.; Thao, N. T.; Wijerathna, H.; Lee, J.; Edussuriya, M.; Choi, D.; Kumar, R. S. In vitro and in vivo anticandidal efficacy of green synthesized gold nanoparticles using Spirulina maxima polysaccharide. *Process Biochem.* **2020**, *92*, 138−148.
(48) Yazdani, S.; Daneshkhah, A.; Diwate, A.; Patel, H.; Smith, J.; Reul, O.; Cheng, R.; Izadian, A.; Hajrasouliha, A. R. Model for gold nanoparticle synthesis: Effect of pH and reaction time. *ACS Omega* **2021**, *6* (26), 16847−16853.

Downloaded from http://pubs.acs.org/ascecg/article-pdf/13/45/19599/4245742/sc5c07786.pdf by UNIV OF OSAKA user on 27 July 2026

(49) Sivaraman, S. K.; Kumar, S.; Santhanam, V. Monodisperse sub-10 nm gold nanoparticles by reversing the order of addition in Turkevich method—The role of chloroauric acid. *J. Colloid Interface Sci.* **2011**, *361* (2), 543−547.
(50) Ramli, M.; Sujoko, I.; Adhha, N.; Annas, D.; Nikmatullah, M.; Ariyanta, H. A.; Apriandanu, D. O. B.; Saputra, I. S.; Khairurrijal, K. Influence of various concentrations of chloroauric acid on the fabrication of gold nanoparticles: Green synthesis using Elaeis guineensis Jacq leaf extract and characterizations. *Results Surf. Interfaces* **2024**, *17*, 100317.
(51) Mountrichas, G.; Pispas, S.; Kamitsos, E. I. Effect of temperature on the direct synthesis of gold nanoparticles mediated by poly (dimethylaminoethyl methacrylate) homopolymer. *J. Phys. Chem. C* **2014**, *118* (39), 22754−22759.
(52) Sardar, R.; Shumaker-Parry, J. S. Spectroscopic and microscopic investigation of gold nanoparticle formation: ligand and temperature effects on rate and particle size. *J. Am. Chem. Soc.* **2011**, *133* (21), 8179−8190.
(53) Ziyue, T.; Chen, W.; Chen, X.; Xia, M.; Chen, Y.; Yang, H.; Chen, H.; Xiaorui, L. Thermal behavior and kinetic mechanism of microalgae and model compounds. *Fuel* **2023**, *344*, 128037.
(54) Zhu, R.-G.; Xiao, H.-Y.; Zhou, Z.; Yin, M.; Xiao, H.; Hu, C.; Wei, G.; Liu, C. Thermal degradation of 18 amino acids during pyrolytic processes. *Sci. Rep.* **2024**, *14* (1), 29192.
(55) Ahmad Kuthi, N.; Chandren, S.; Basar, N.; Jamil, M. S. S. Biosynthesis of gold nanoisotrops using Carallia brachiata leaf extract and their catalytic application in the reduction of 4-nitrophenol. *Front. Chem.* **2022**, *9*, 800145.
(56) Aji, A.; Gulo, S. R.; Saputra, M. Y.; Putri, R. A.; Nareswari, T. L.; Sukrasno; Amin, A. K. Gold Nanoparticles Derived from Acacia mangium: Optimized Synthesis, Physicochemical Properties, and Bioactivity. *J. Inorg. Organomet. Polym. Mater.* **2025**, *35*, 5345−5362.
(57) Mares Briones, F.; Frutis-Murillo, M.; López-Miranda, J.; López Meza, J.; Rosas, G.; Estevez, M.; Esparza, R. Effect of Sargassum-mediated synthesis on hemolytic activity of Au nanoparticles. *MRS Adv.* **2024**, *10*, 30−35.
(58) Bogireddy, N.; Pal, U.; Gomez, L. M.; Agarwal, V. Size controlled green synthesis of gold nanoparticles using Coffea arabica seed extract and their catalytic performance in 4-nitrophenol reduction. *RSC Adv.* **2018**, *8* (44), 24819−24826.
(59) Ennaceri, H.; Mkpuma, V. O.; Amo-Duodu, G.; Menkiti, M.; Ishika, T.; Vadiveloo, A.; Moheimani, N. R. Microalgae as sustainable bio-factories for nanoparticle biosynthesis: Progress and challenges. *Bioresour. Technol. Rep.* **2025**, *30*, 102089.
(60) Premarathna, A. D.; Ahmed, T. A.; Kulshreshtha, G.; Humayun, S.; Darko, C. N. S.; Rjabovs, V.; Hammami, R.; Critchley, A. T.; Tuvikene, R.; Hincke, M. T. Polysaccharides from red seaweeds: Effect of extraction methods on physicochemical characteristics and antioxidant activities. *Food Hydrocolloids* **2024**, *147*, 109307.
(61) Dejsungkranont, M.; Chen, H.-H.; Sirisansaneeyakul, S. Enhancement of antioxidant activity of C-phycocyanin of Spirulina powder treated with supercritical fluid carbon dioxide. *J. Agric. Nat. Resour.* **2017**, *51* (5), 347−354.
(62) Wu, L.-c.; Ho, J.-a. A.; Shieh, M.-C.; Lu, I.-W. Antioxidant and antiproliferative activities of Spirulina and Chlorella water extracts. *J. Agric. Food Chem.* **2005**, *53* (10), 4207−4212.
(63) Toshkova-Yotova, T.; Pilarski, P.; Yocheva, L.; Petrova, D.; Chaneva, G. Screening of antimicrobial and antioxidant properties of green microalga Coelastrella sp. BGV. *Oxid. Commun.* **2020**, *43* (2), 265−279.
(64) Ferreira, G.; Pinto, L. F. R.; Filho, R. M.; Fregolente, L. A review on lipid production from microalgae: Association between cultivation using waste streams and fatty acid profiles. *Renewable Sustainable Energy Rev.* **2019**, *109*, 448−466.
(65) Agarwal, A.; Jeevanandham, S.; Sangam, S.; Chakraborty, A.; Mukherjee, M. Exploring the role of carbon-based nanomaterials in microalgae for the sustainable production of bioactive compounds and beyond. *ACS Omega* **2022**, *7* (26), 22061−22072.
(66) Deyab, M. A.; El-Sheekh, M. M.; Hasan, R. S.; Elsadany, A. Y.; Abu Ahmed, S. E.-S. Phytochemical Components of two Cyano-bacterial local strains. *Sci. J. Damietta Fac. Sci.* **2021**, *11* (1), 67−75.
(67) Femina Carolin, C.; Kamalesh, T. Advances in stabilization of metallic nanoparticle with biosurfactants-A review on current trends. *Heliyon* **2024**, *10*, No. e29773.
(68) Douliez, J.-P.; Novales, B.; Gaillard, C. Synthesising gold nanoparticles within bola fatty acid nanosomes. *J. Colloid Interface Sci.* **2009**, *337* (2), 610−613.
(69) Nguyen, M. T.; Wongrujipairoj, K.; Tsukamoto, H.; Kheawhom, S.; Mei, S.; Aupama, V.; Yonezawa, T. Synergistic effect of the oleic acid and oleylamine mixed-liquid matrix on particle size and stability of sputtered metal nanoparticles. *ACS Sustainable Chem. Eng.* **2020**, *8* (49), 18167−18176.
(70) Das, R.; Nath, S. S.; Bhattacharjee, R. Preparation of linoleic acid capped gold nanoparticles and their spectra. *Phys. E* **2010**, *43* (1), 224−227.
(71) Wang, Y.; Gao, Z.; Han, Z.; Liu, Y.; Yang, H.; Akkin, T.; Hogan, C. J.; Bischof, J. C. Aggregation affects optical properties and photothermal heating of gold nanospheres. *Sci. Rep.* **2021**, *11* (1), 898.

Downloaded from http://pubs.acs.org/ascecg/article-pdf/13/45/19599/4245742/sc5c07786.pdf by UNIV OF OSAKA user on 27 July 2026

https://doi.org/10.1021/acssuschemeng.5c07786
ACS Sustainable Chem. Eng. 2025, 13, 19599−19612